

Strong magnetoresistance modulation by Ir insertion in a Ta/Ir/CoFeB trilayerR. Q. Zhang ¹, L. Y. Liao,¹ X. Z. Chen,¹ H. Q. Wu,² F. Pan,¹ and C. Song ^{1,*}¹Key Laboratory of Advanced Materials (MOE), School of Materials Science and Engineering, Tsinghua University, Beijing 100084, China²Institute of Microelectronics, Tsinghua University, Beijing 100084, China

(Received 28 July 2019; revised manuscript received 28 September 2019; published 17 October 2019)

The spin-orbit torque (SOT) switching of trilayers with two heavy-metal layers on the same side of the ferromagnetic metal layer was studied, realizing tunable spin Hall angle, domain-wall motion, and Dzyaloshinskii-Moriya interaction. However, systematic research on the magnetoresistance in such structures is still lacking. In this work, we investigate the anisotropic magnetoresistance (AMR) and the spin Hall magnetoresistance (SMR) by inserting an ultrathin Ir layer ($t_{\text{Ir}} \leq 1.4$ nm) into Ta/CoFeB. The Ir layer with the thickness larger than 0.4 nm can transform the AMR from positive to negative, which is attributed to the electronic structure of Ir. This process realizes the interfacial modulation of AMR, which is generally considered as a bulk property. The SMR ratio decreases first and then increases with increasing Ir thickness, producing the minimum and maximum at $t_{\text{Ir}} = 0.3$ nm and $t_{\text{Ir}} = 0.9$ nm, respectively, which reflects the ultrasmall spin-diffusion length (<0.5 nm) and strong spin-memory loss in Ir. Further analyses combined with the SOT switching measurements unravel the existence of the anomalous Hall magnetoresistance, implying the non-negligible spin accumulation due to the anomalous Hall effect of the ferromagnetic metal. The combination of a large negative AMR and comparatively smaller SMR results in a negative planar Hall resistance. Our findings enrich the understanding of the magnetoresistances of heavy-metal/ferromagnetic metal trilayer systems.

DOI: [10.1103/PhysRevB.100.144425](https://doi.org/10.1103/PhysRevB.100.144425)**I. INTRODUCTION**

The spin-orbit torque (SOT) in heavy-metal (HM)/ferromagnetic metal (FM) bilayers has been extensively studied due to its ability to manipulate magnetic dynamics and switch the uniform magnetization, where the large spin-orbit coupling of the HM plays a central role for the understanding of spin-current generation, domain-wall motion, and Dzyaloshinskii-Moriya interaction [1–5]. Recently, it was found that the SOT polarity and efficiency can be largely modulated by employing two HM layers on the same side of the FM layer, showing strong tunability of the phenomena mentioned above [6–8]. Considering that different HMs contribute differently on the electric conductivity and spin-current generation, the magnetoresistance is expected to show novel characteristics in HM/FM trilayers, which in turn could help deepen the understanding of the charge and spin transport in such structures. Anisotropic magnetoresistance (AMR) is a prominent feature of ferromagnetic materials where the magnetoresistance depends on the relative direction between the magnetization and the current [9,10]. For most of the ferromagnetic materials, the resistivity of the current parallel to the magnetization case is larger than that of the perpendicular case, which is defined as the positive AMR, while some ferromagnetic compounds and half metals were found to have negative AMR [11–14]. Although AMR is a bulk property and is an *intrinsic* character of a magnetic material itself, when contacted with a HM, the additional interface creates new electron scattering chances, which will

possibly strongly affect the AMR ratio and even AMR sign. This *extrinsic* modulation of AMR is of interest.

Contrary to AMR, spin Hall magnetoresistance (SMR) is a typical interface-dependent spin phenomenon, because it highly relies on the spin accumulation at the HM/FM interface [15,16]. SMR was first demonstrated in a HM/ferromagnetic insulator (FI) bilayer [15,17], where the longitudinal conductivity enhancement due to the spin Hall effect and inverse spin Hall effect is maximized (minimized) when the magnetization of FI is parallel (perpendicular) to the spin polarization σ . Compared with FI which could only absorb the transverse spin current, the ability of a FM to absorb the longitudinal spin current results in a remarkably increased SMR in HM/FM systems [18]. In a HM/FM trilayer, the two HM layers have different ability to generate and transport spin current, thus the change of relative thickness of the two HM layers would have a large impact on the SMR phenomenon. Recently, Luan *et al.* [19] reported that the SMR ratio could be enhanced by capping a thin W layer onto yttrium iron garnet (YIG)/Pt, which is unexpected since W and Pt have opposite spin Hall angle and are supposed to suppress the spin accumulation. Therefore, the SMR in HM/FM trilayers is not so accessible and more research is needed.

The experiments below demonstrate that both AMR and SMR can be significantly manipulated by inserting an ultrathin Ir layer into Ta/CoFeB. The extrinsic modulation of the AMR ratio and even the sign is clearly unraveled, and the Ir thickness dependence of SMR reflects the ultrasmall spin-diffusion length and strong spin-memory loss in Ir. Further analyses with the SOT switching measurements indicate the existence of the recently demonstrated anomalous Hall magnetoresistance (AHMR) [20]. By combining the AMR

*songcheng@mail.tsinghua.edu.cn

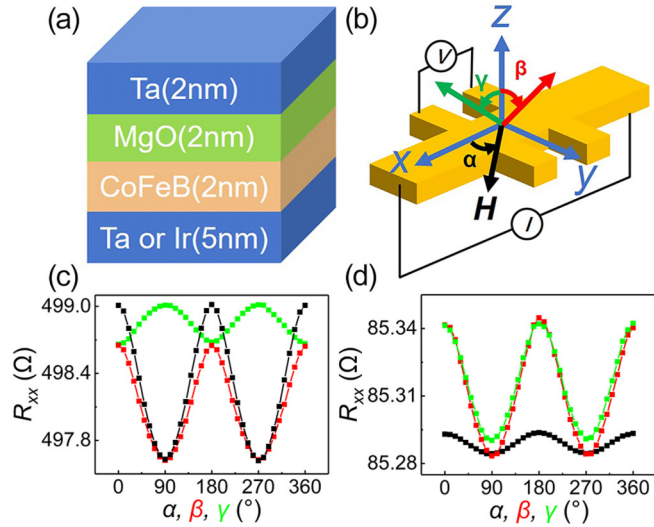


FIG. 1. Schematic of (a) control sample layout and (b) measurement coordinate. Angular dependence of R_{xx} as magnetic field rotated in xy (α scan, black line), yz (β scan, red line), and xz (γ scan, green line) plane, respectively, for (c) Ta/CoFeB and (d) Ir/CoFeB.

and the SMR of the Ta/Ir/CoFeB trilayer, an extraordinary negative planar Hall resistance is obtained.

II. EXPERIMENTAL

Stacks of Ta(5)/Ir(t_{Ir})/CoFeB(2)/MgO(2)/Ta(2) ($t_{Ir} = 0 \sim 1.4$, units in nanometer from the bottom to top, referred to as Ta/Ir(t_{Ir})/CoFeB) were deposited on thermally oxidized Si substrates via magnetron sputtering at a base vacuum of 5×10^{-6} Pa. The deposition rates for Ta, Ir, CoFeB, and MgO are 0.15, 0.15, 0.12, and 0.04 Å/s, respectively. Films were annealed at 300 °C for half an hour with an in-plane magnetic field of 0.7 T. After that, Hall bar devices were fabricated by lithography and Ar-ion etching. The width of current channel is 20 μm , and the distance between voltage probes that measure the longitudinal resistance (R_{xx}) is 30 μm . Then the Ti(10)/Au(100) electrodes were prepared by e-beam evaporation and lift-off process. All of the magnetoresistance measurements were carried out at 300 K by four-probe method with a current of 0.2 mA.

III. RESULTS AND DISCUSSION

We first show magnetoresistance results for two control samples, Ta(5)/CoFeB(2)/MgO(2)/Ta(2) and Ir(5)/CoFeB(2)/MgO(2)/Ta(2) (referred to as Ta/CoFeB and Ir/CoFeB, respectively). The sample layout is shown in Fig. 1(a). R_{xx} was recorded while rotating the magnetic field in three typical planes, i.e., xy , yz , and xz planes, and the definitions of α , β , and γ are highlighted in the schematic in Fig. 1(b). The magnetic field was kept at 2 T which is larger than the anisotropy field during all of the measurements, ensuring that the magnetization (M) direction of CoFeB can be arranged collinear to the magnetic-field direction. Generally, the AMR and SMR can be separated by different measurement configurations [15,21,22]: during the β scan, M remains orthogonal to the current I , thus the

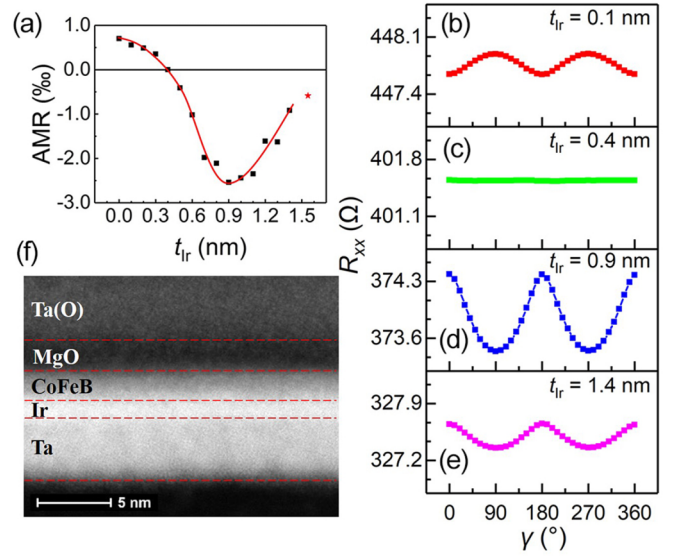


FIG. 2. (a) t_{Ir} dependence of AMR ratio. The red line is a guide to the eyes. Angular (γ) dependence of R_{xx} for (b) $t_{Ir} = 0.1$ nm, (c) $t_{Ir} = 0.4$ nm, (d) $t_{Ir} = 0.9$ nm, and (e) $t_{Ir} = 1.4$ nm, respectively. (f) HAADF-STEM image of Ta/Ir(0.9)/CoFeB.

change of R_{xx} mainly reflects the SMR, while for the γ scan, σ remains orthogonal to I , thus the change of R_{xx} reflects the AMR. However, this method is not valid if the FM becomes crystalline or textured because of extra contribution to the β -scan signal [23–25]. Since our sputtered films are amorphous (see Supplemental Material [26]), it is convenient to distinguish AMR and SMR signals in this work. The angular dependence of R_{xx} for Ta/CoFeB and Ir/CoFeB are displayed in Figs. 1(c) and 1(d), respectively. Both samples show obvious SMR behaviors (β -scan), which are as expected because the large spin-orbit coupling in Ta and Ir guarantees the considerable spin Hall effect and resultant spin-current generation. However, the signs of AMR in two samples are opposite (γ scan). To be specific, the sign of AMR in Ir/CoFeB is negative as shown in the γ -scan curve in Fig. 1(d), i.e., R_{xx} for I parallel to the M case is smaller than the perpendicular case: ($R_{//}[R_{xx}(\gamma = 90^\circ)] < R_{\perp}[R_{xx}(\gamma = 0^\circ)]$). This kind of sizable negative AMR was only found in some specific ferromagnets previously [11–14]. The possible mechanism for this unusual AMR will be discussed later.

We now focus on the effect of the Ir insertion on the AMR in the series of Ta/Ir(t_{Ir})/CoFeB samples. Here we define the AMR ratio as $(R_{//}[R_{xx}(\gamma = 90^\circ)] - R_{\perp}[R_{xx}(\gamma = 0^\circ)]) / R_{\perp}[R_{xx}(\gamma = 0^\circ)]$. Figure 2(a) summarizes the t_{Ir} dependence of AMR, and the Ta/CoFeB case is also included (e.g., $t_{Ir} = 0$). With the increase of t_{Ir} , the AMR ratio monotonically decreases and reaches near zero at $t_{Ir} = 0.4$ nm. After that, the sign of AMR ratio changes, while the magnitude keeps increasing until $t_{Ir} = 0.9$ nm. Further increase of t_{Ir} results in a sharp decrease in the AMR ratio, which approaches that of Ir/CoFeB [denoted by the red star in Fig. 2(a)]. The most dramatic feature here is that the AMR sign transitions from positive to negative once t_{Ir} is larger than a small thickness of 0.4 nm. To show the details, four specific AMR curves with $t_{Ir} = 0.1$,

0.4, 0.9, and 1.4 nm, respectively, are shown in Figs. 2(b), 2(c), 2(d), and 2(e), for which the AMR ratio gets the largest positive value, near zero, the maximum negative value, and close to the Ir/CoFeB case, respectively. This t_{Ir} -dependent AMR ratio clearly reveals the extrinsic modulation of AMR.

A previous study based on the improved two-current model demonstrated that the AMR effect strongly depends on s - d scattering processes from the conduction state to the localized d states [27]. The AMR ratio is proportional to $A(D_{\uparrow}^{(d)} - D_{\downarrow}^{(d)})(1/\rho_{\downarrow} - 1/\rho_{\uparrow})$, where $A = 3/4(B/H_{\text{ex}})^2$ with B the spin-orbit coupling constant and H_{ex} the exchange field of the localized d states, $D_{\sigma}^{(d)}$ ($\sigma = \uparrow$ or \downarrow) is the density of states (DOS) of d state of the σ spin at Fermi energy, and ρ_{σ} corresponds approximately to the resistivity of the conductive σ spin (mainly the s state). According to this simple model, the sign of AMR ratio is determined by the relative magnitude of $D_{\uparrow}^{(d)}$ and $D_{\downarrow}^{(d)}$, as well as ρ_{\uparrow} and ρ_{\downarrow} . For instance, Fe_4N has negative AMR ratio because of $D_{\uparrow}^{(d)} < D_{\downarrow}^{(d)}$ and $\rho_{\uparrow} > \rho_{\downarrow}$ [27]. Although this model is based on the pure ferromagnet cases, we could utilize it to qualitatively explain the AMR in the present HM/FM system. When two solid films contact with each other, the band structure will rearrange to a new balance state. Since the mean-free path of electrons are usually several nanometers or larger, the s state of one layer can be scattered by the d state of the adjacent layer. Therefore, the two thin metal layers can be treated as a whole from the viewpoint of the s - d scattering process. The additional HM layer is possible to influence the AMR ratio in three ways: (i) The d states of HM provide extra scattering centers for the conductive electrons, meanwhile HM usually has large spin-orbit coupling; (ii) Some of the HMs have non-negligible magnetic proximity effect (MPE), resulting in the spin splitting and unequal DOS for \uparrow and \downarrow spins of the HM at the Fermi level; (iii) The resistivity of conductive spins in HM and FM may be seriously different, and the shunting effect of HM also affects the “apparent” AMR ratio. All of these factors can have potential influence on the magnitude and even the sign on the AMR ratio.

Taking these factors into account, our experimental results can be qualitatively understood. First we focus on the size of AMR ratio in Ta/CoFeB and Ir/CoFeB. Since the AMR ratio is approximately inversely proportional to the resistivity of conductive spin states (ρ_{σ}), R_{xx} is an important parameter which can influence the AMR ratio. As can be seen in Figs. 1(c) and 1(d), R_{xx} of Ta/CoFeB and Ir/CoFeB with the same thickness are obviously different. This is true based on the common sense that the conductivity of Ir should be much larger than that of Ta. The low resistivity of Ir conductive spin states would contribute greatly to the AMR ratio. Consequently, even though the shunting effect of Ir is more serious than that of Ta, the AMR ratio of Ir/CoFeB (-5.86×10^{-4}) is still comparable to that of Ta/CoFeB (7.02×10^{-4}). According to this deduction, the small AMR ratios in previously reported HM/FM bilayers [18,28,29] are all comprehensible taking the large longitudinal resistivity into account.

We now discuss the sign change of AMR in Ta/Ir(t_{Ir})/CoFeB series of samples. The basis of this analysis is that Ir/CoFeB has negative AMR. CoFeB itself possesses positive AMR (see Supplemental Material [26]). With the

introduction of Ir, the relative magnitude of either $D_{\uparrow}^{(d)}$ and $D_{\downarrow}^{(d)}$ or ρ_{\uparrow} and ρ_{\downarrow} must change, causing the sign reversal of AMR. Notice that Ir is a HM which possesses MPE [30,31]. If the induced magnetic moment in Ir caused an opposite relative magnitude of $D_{\uparrow}^{(d_{\text{Ir}})}$ and $D_{\downarrow}^{(d_{\text{Ir}})}$ with that of CoFeB, there would be a chance that $D_{\uparrow}^{(d)} - D_{\downarrow}^{(d)}$ changes sign, accompanied by the sign reversal of the AMR. Therefore, the MPE of Ir is likely to be the origin of the negative AMR in Ir/CoFeB. Based on the s - d scattering model, the electronic structure of Ir should have some unique characteristics, leading to the unusual s - d scattering process in Ir/CoFeB. It was previously reported that in epitaxial Fe/Pt bilayer, AMR is significantly enhanced due to induced magnetization of Pt in the conduction band, which is caused by the spin-dependent scattering from Fe [25]. However, this cannot be the mechanism of our case since the spin-diffusion length of HM should determine the thickness limit of HM which can enhance AMR, while the size of AMR in Ta/Ir(t_{Ir})/CoFeB keeps increasing even when t_{Ir} is much larger than its spin-diffusion length (~ 0.5 nm; see Refs. [32,33] and the discussion below about the SMR results). Meanwhile it was reported that several atomic percentages of Ir-doped Co, Fe, and Ni exhibit a large negative AMR [11]. The bilayer case may have similar physical origin with that of the alloy case. In a word, the existence of an Ir layer adjacent to CoFeB tends to modulate the AMR from positive to negative. With the increase of t_{Ir} until 0.9 nm, the negative influence of Ir manifests gradually, making the AMR ratio decrease and then change sign. The reduced AMR value after t_{Ir} reaches 0.9 nm is due to the large shunting effect of Ir. One may doubt that the ultrathin Ir layer becomes alloying with CoFeB after annealing, so that our result would have no difference from the previous alloy case. To eliminate this possibility, the high-angle annular dark-field-scanning transmission electron microscopy (HAADF-STEM) was used to provide the interfacial quality of Ta/Ir(0.9)/CoFeB, which has the largest negative AMR ratio. Corresponding cross-sectional image is displayed in Fig. 2(f). Despite the fact that some interfacial diffusion cannot be completely excluded, the image shows clear layer-by-layer structure, indicating the alloying between Ir and CoFeB is not dominant. It is then concluded that our observation reveals the effective interfacial modulation of the AMR.

Compared with the AMR results, the SMR ratio which is defined as $[R_{xx}(\beta = 0^\circ) - R_{xx}(\beta = 90^\circ)]/R_{xx}(\beta = 90^\circ)$ has different tendency with respect to t_{Ir} , as presented in Fig. 3(a). Remarkably, there is no sign transition, but t_{Ir} plays a fundamental role on the magnitude of SMR. With the increase of t_{Ir} from 0 to 0.3 nm, the SMR ratio decreases to a minimal value, then increases until t_{Ir} reaches 0.9 nm. After that, the SMR ratio falls again. SMR curves for the minimum and maximum SMR ratio at $t_{\text{Ir}} = 0.3$ nm and $t_{\text{Ir}} = 0.9$ nm, respectively, are shown in Figs. 3(c) and 3(d), and the smallest and largest t_{Ir} case ($t_{\text{Ir}} = 0.1$ nm and 1.4 nm, respectively) are included in Figs. 3(b) and 3(e).

In order to analyze this change process, the most crucial physical quantities are the spin Hall angle (θ_{SH}) and the spin-diffusion length (λ) of the HM [16]. θ_{SH} is defined as the ratio of the spin current to the charge current, which also reflects the amount of spin accumulation at the HM/FM interface. A

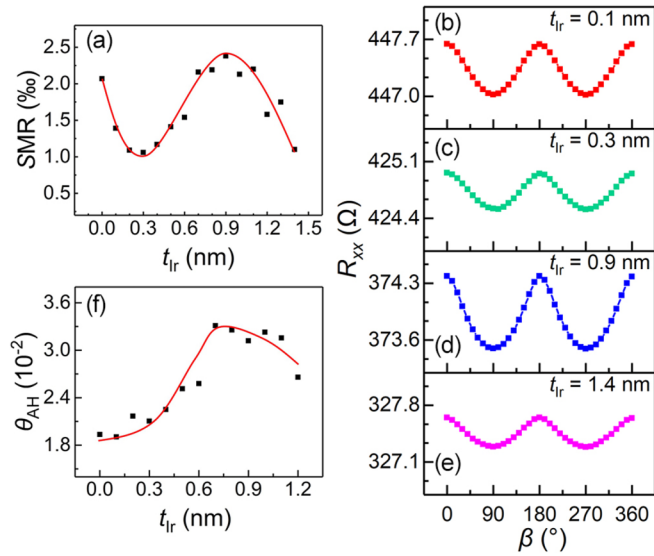


FIG. 3. (a) t_{Ir} dependence of SMR ratio. Angular (β) dependence of R_{xx} for (b) $t_{\text{Ir}} = 0.1$ nm, (c) $t_{\text{Ir}} = 0.3$ nm, (d) $t_{\text{Ir}} = 0.9$ nm, and (e) $t_{\text{Ir}} = 1.4$ nm, respectively. (f) t_{Ir} dependence of θ_{AH} . The red lines are a guide to the eyes.

previous model predicted that the magnitude of SMR scales with the square of θ_{SH} [16,22]. λ is a parameter determining the HM thickness dependence of SMR (i.e., the peak value). In general, the maximum SMR appears at about 2λ of the HM thickness [5,16]. As for our Ta/Ir/CoFeB case, the peak value is roughly 0.9 nm, thus λ of Ir (λ_{Ir}) is deduced to be smaller than 0.5 nm. In this case, the SMR ratio decreases when t_{Ir} is beyond 0.9 nm because the extra part of Ir does not contribute to the SMR but only has shunting effect. Such a small λ_{Ir} is consistent with the recent reported results utilizing spin pumping [32,33]. Furthermore, the SMR ratio achieves a minimum at $t_{\text{Ir}} = 0.3$ nm. The reduced SMR ratio from $t_{\text{Ir}} = 0$ to $t_{\text{Ir}} = 0.3$ nm is attributed to the opposite θ_{SH} of Ta and Ir ($\theta_{\text{SH}}^{\text{Ta}}$ and $\theta_{\text{SH}}^{\text{Ir}}$, respectively) [34], which causes a counteraction of spin-current accumulation at the Ir/CoFeB interface. Here what is unexpected is that the minimum value takes place at such a small t_{Ir} since $\theta_{\text{SH}}^{\text{Ta}}$ should be several times larger than $\theta_{\text{SH}}^{\text{Ir}}$ [5,35,36]. But, note that the conductivity of Ir is much larger than Ta, resulting in a much larger electric current density in Ir, and the contribution of Ir to the spin current is magnified. Meanwhile, the ultrasmall λ and strong spin-memory loss in Ir [33] lead to that the spin current of Ta is difficult to “pass through” the Ir layer [37].

To further understand the spin accumulation and transport in this trilayer system, we did the SOT switching measurements in perpendicular magnetized Ta/Ir(t_{Ir})/CoFeB(1.1) series of Hall crosses with the current channel width of 3 μm . Only the samples with $t_{\text{Ir}} = 0 \sim 0.9$ nm are shown, because the perpendicular magnetic anisotropy cannot maintain if t_{Ir} is further increased. Figure 4(a) summarizes the critical current of switching CoFeB from down magnetization to up magnetization with a positive external field of 200 Oe. With increasing t_{Ir} , the critical current also increases, for which the SOT switching curves of $t_{\text{Ir}} = 0$ and $t_{\text{Ir}} = 0.4$ nm samples are presented in Figs. 4(b) and 4(c), respectively, indicating

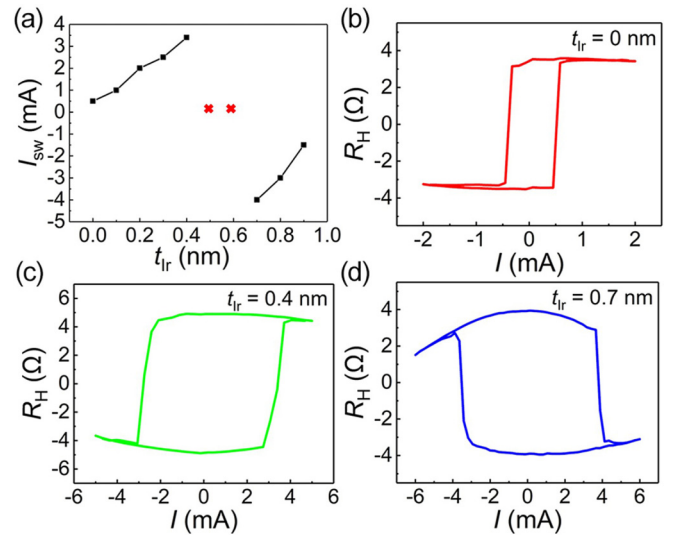


FIG. 4. (a) t_{Ir} dependence of the critical current to switch CoFeB from down magnetization to up magnetization under a positive external field of 200 Oe for perpendicular magnetized Ta/Ir(t_{Ir})/CoFeB(1.1) samples. Typical SOT switching curves represented by Hall resistance for (b) $t_{\text{Ir}} = 0$ nm, (c) $t_{\text{Ir}} = 0.4$ nm, and (d) $t_{\text{Ir}} = 0.7$ nm, respectively.

the decrease of net spin current acting on CoFeB due to the opposite θ_{SH} of Ir to Ta. At $t_{\text{Ir}} = 0.5$ and 0.6 nm, magnetization switching behavior is unrealizable until the applied current is too large and destroys the devices (even when we use a positive external field of 2 kOe which should decrease the critical switching current greatly), which means that the net spin accumulation at Ir/CoFeB interface is negligible. The situation turns out to be different for the $t_{\text{Ir}} = 0.7$ nm case. Magnetization switching can be achieved again but with an opposite polarity, implying Ir starts to play a dominant role and the apparent sign of θ_{SH} changes, as illustrated in Fig. 3(d). The ultrasmall t_{Ir} at which the SOT switching polarity changes its sign also supports the ultrasmall spin-diffusion length and strong spin-memory loss in Ir.

According to the SOT switching results, the spin-current compensation point is around $t_{\text{Ir}} = 0.5$ nm. However, t_{Ir} for the minimum SMR ratio is 0.3 nm, and the SMR ratio at $t_{\text{Ir}} = 0.5$ nm is quite sizable. This is somehow confusing since a small SMR ratio is expected when the spin current of Ta and Ir is nearly compensated. In $\text{Pt}_x\text{Ta}_{1-x}/\text{YIG}$ bilayer, when the effective spin Hall angle vanishes, the SMR also disappears [38]. Notice that the biggest difference with the $\text{Pt}_x\text{Ta}_{1-x}/\text{YIG}$ is that the CoFeB layer is also conductive and can contribute to the total magnetoresistance, so the so-called SMR in the discussions above may have contributions from other physical effects. An Fe single layer was reported to exhibit the same angular dependence of magnetoresistance compared with SMR [24], and until recently the physical origin of this magnetoresistance was clarified as the anomalous Hall effect (AHE) of the ferromagnet [20]. To test whether this AHMR exists in our case, we did the β scan for a single 2-nm-thick CoFeB layer (protected by MgO and Ta). Unfortunately, a magnetoresistance with opposite sign to SMR was observed (see Supplemental Material [26]). This means that the AHMR

of CoFeB single layer is masked by the geometric size effect due to its relatively weak AHE [20]. However, when contacted with HM, the AHE of FM could be enhanced greatly due to the large spin-orbit coupling of HM [39]. Figure 3(f) displays the t_{Ir} dependence of the anomalous Hall angle (ϑ_{AH}) which is defined as $\rho_{\text{AH}}/\rho_{\text{xx}}$, where ρ_{AH} and ρ_{xx} are the anomalous Hall resistivity and longitudinal resistivity, respectively. The deduction of ρ_{AH} can be found in Supplemental Material [26]. With the increase of t_{Ir} until t_{Ir} reaches 0.7 nm, ϑ_{AH} increases significantly, implying that the additional Ir layer strongly strengthens the AHE by the extrinsic scattering mechanism. It is worthy pointing out that ϑ_{AH} of Ta/Ir(t_{Ir})/CoFeB series of samples are several times larger than the CoFeB single layer [40,41], and comparable to $\text{Fe}_{1-x}\text{Pt}_x$ which shows remarkable AHMR [20]. While the AHMR ratio is proportional to the strength of the AHE, a non-negligible AHMR is highly proposed in Ta/Ir(t_{Ir})/CoFeB series of samples. Therefore, at a relatively thin t_{Ir} range, the AHMR ratio should increase monotonously while the real SMR ratio decreases first and then increases. A combination of these two phenomena causes the measured t_{Ir} for the minimum SMR ratio (0.3 nm) to be smaller than that of the spin-current compensation point (0.5 nm). Despite that our experimental observations can be explained taking AHMR into account, there are still other possible mechanisms which may be responsible for the results, e.g., the recently demonstrated spin-orbit magnetoresistance (SOMR) [42,43]. The inserted Ir layer could provide large Rashba spin-orbit coupling at the interface which is correlated to the SOMR, while the experimental identification is difficult because the ultrasmall spin-diffusion length of Ir makes it hard to distinguish SOMR out of SMR through thickness-dependence measurements [43]. Further studies on β -scan magnetoresistance in multilayers containing conductive ferromagnetic layer are needed. To simplify, we just keep the concept of SMR for β scan in this paper.

The discussions of AMR and SMR above emphasize the different physical origins of these two magnetoresistances. A detailed inspection on the magnitude of AMR and SMR in our Ta/Ir(t_{Ir})/CoFeB system shows that the AMR ratio is comparable to the SMR ratio in some cases, which is unusual for the HM/FM structures [18,28,29]. This can also be reflected in the α -MR ratio when rotating the magnetic field in the xy plane, which we define as $[R_{\text{xx}}(\alpha = 0^\circ) - R_{\text{xx}}(\alpha = 90^\circ)]/R_{\text{xx}}(\alpha = 90^\circ)$, as presented in Fig. 5(a). For this α scan, the change in R_{xx} is the combined effect of AMR and SMR, and the α -MR ratio is approximately equal to the AMR ratio plus the SMR ratio. When t_{Ir} increases, the α -MR ratio decreases gradually, and unexpectedly the sign becomes opposite at $t_{\text{Ir}} = 0.9 \sim 1.1$ nm. Then the α -MR ratio returns to positive again, whereas the size remains small. It is the competing between AMR and SMR that leads to this result. Since the planar Hall effect is the transverse counterpart of this α -MR, one could expect that the planar Hall resistance (R_{PHE}) should also be negative at $t_{\text{Ir}} = 0.9 \sim 1.1$ nm, and we demonstrate it true. Figure 5(b) lists R_{PHE} as a function of t_{Ir} , which is strongly correlated to the α -MR. The detailed process for obtaining R_{PHE} can be found in Supplemental Material [26]. So far, according to the different relative magnitude of R_{L} , R_{T} , and R_{\perp} , where R_{L} and R_{T} are R_{xx} with in-plane field parallel and perpendicular to I , respectively, and R_{\perp} is R_{xx}

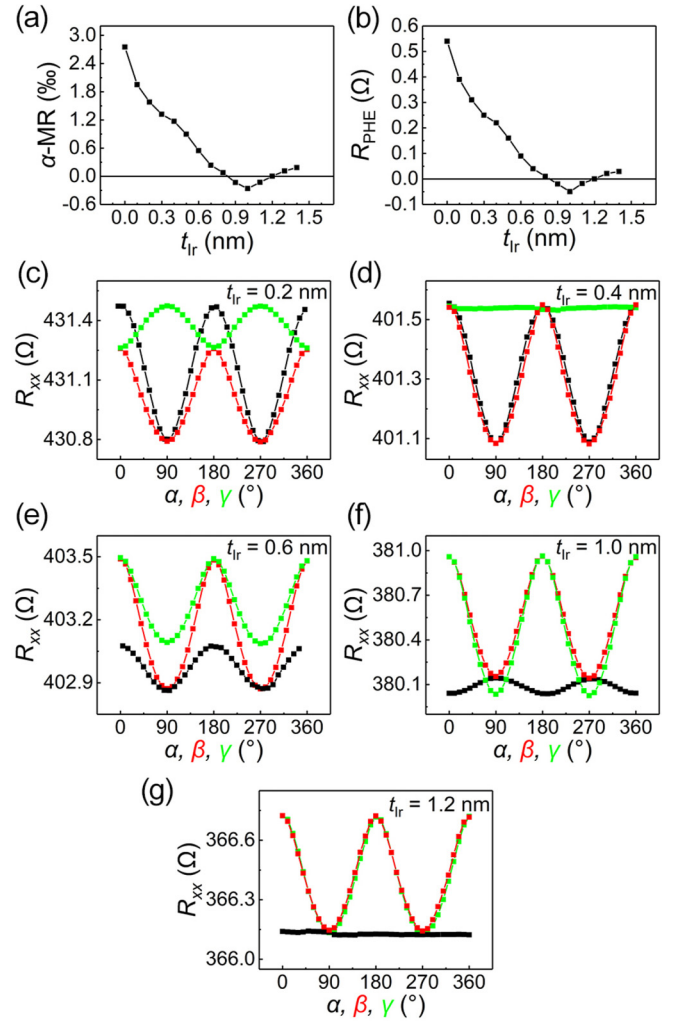


FIG. 5. t_{Ir} dependence of (a) the α -MR and (b) R_{PHE} . Typical magnetoresistance curves for (c) $t_{\text{Ir}} = 0.2$ nm, (d) $t_{\text{Ir}} = 0.4$ nm, (e) $t_{\text{Ir}} = 0.6$ nm, (f) $t_{\text{Ir}} = 1.0$ nm, and (g) $t_{\text{Ir}} = 1.2$ nm.

with out-of-plane field, the magnetoresistance behaviors for the Ta/Ir(t_{Ir})/CoFeB series of samples can be divided into five types: (i) $R_{\text{L}} > R_{\text{T}} > R_{\perp}$ for $t_{\text{Ir}} = 0.1 \sim 0.3$ nm, with positive AMR; (ii) $R_{\text{L}} \approx R_{\perp} > R_{\text{T}}$ for $t_{\text{Ir}} = 0.4$ nm, with a near-zero AMR ratio; (iii) $R_{\perp} > R_{\text{L}} > R_{\text{T}}$ for $t_{\text{Ir}} = 0.5 \sim 0.8$ nm, with the AMR ratio transformed to negative; (iv) $R_{\perp} > R_{\text{T}} > R_{\text{L}}$ for $t_{\text{Ir}} = 0.9 \sim 1.1$ nm, with negative R_{PHE} ; (v) $R_{\perp} > R_{\text{L}} \approx R_{\text{T}}$ for $t_{\text{Ir}} = 1.2$ nm, with a near-zero R_{PHE} . Each type is given a detailed example as shown in Figs. 5(c)–5(g). The rich varieties of magnetoresistances due to the Ir insertion in Ta/CoFeB are clearly demonstrated.

IV. CONCLUSIONS

In conclusion, by studying the magnetoresistances in Ta/Ir(t_{Ir})/CoFeB series of samples, we demonstrate strong modulation of both AMR and SMR. The rich varieties of both the magnitude and the sign of AMR show extrinsic tunability of AMR, where the electronic structure of Ir plays a significant role. The SMR data together with the SOT measurements reflect an ultrasmall spin-diffusion length and strong spin-

memory loss in Ir. This finding also emphasizes the importance of the AHE-related AHMR in this angular-dependent analysis. Furthermore, utilizing the large negative AMR and a SMR with a smaller value, a negative R_{PHE} is realized. Our research deepens the understanding of magnetoresistances in HM/FM trilayer systems, and may inspire further work on the theoretical calculations.

ACKNOWLEDGMENTS

C.S. acknowledges the support of Beijing Innovation Center for Future Chip (ICFC) and Young Chang Jiang Scholars Program. This work is supported by the National Key R&D Program of China (Grant No. 2017YFB0405704) and National Natural Science Foundation of China (Grants No. 51871130, No. 51571128, and No. 51671110).

- [1] L. Liu, O. J. Lee, T. J. Gudmundsen, D. C. Ralph, and R. A. Buhrman, *Phys. Rev. Lett.* **109**, 096602 (2012).
- [2] J. Kim, J. Sinha, M. Hayashi, M. Yamanouchi, S. Fukami, T. Suzuki, S. Mitani, and H. Ohno, *Nat. Mater.* **12**, 240 (2013).
- [3] S. Emori, U. Bauer, S.-M. Ahn, E. Martinez, and G. S. D. Beach, *Nat. Mater.* **12**, 611 (2013).
- [4] M. Belmeguenai, J.-P. Adam, Y. Roussigné, S. Eimer, T. Devolder, J.-V. Kim, S. M. Cherif, A. Stashkevich, and A. Thiaville, *Phys. Rev. B* **91**, 180405(R) (2015).
- [5] Y. Ishikuro, M. Kawaguchi, N. Kato, Y.-C. Lau, and M. Hayashi, *Phys. Rev. B* **99**, 134421 (2019).
- [6] P. He, X. Qiu, V. L. Zhang, Y. Wu, M. H. Kuok, and H. Yang, *Adv. Electron. Mater.* **2**, 1600210 (2016).
- [7] Q. Ma, Y. Li, D. B. Gopman, Y. P. Kabanov, R. D. Shull, and C. L. Chien, *Phys. Rev. Lett.* **120**, 117703 (2018).
- [8] Y. Chen, Q. Zhang, J. Jia, Y. Zheng, Y. Wang, X. Fan, and J. Cao, *Appl. Phys. Lett.* **112**, 232402 (2018).
- [9] T. R. McGuire and R. I. Potter, *IEEE Trans. Magn.* **11**, 1018 (1975).
- [10] Y. Y. Wang, C. Song, B. Cui, G. Y. Wang, F. Zeng, and F. Pan, *Phys. Rev. Lett.* **109**, 137201 (2012).
- [11] T. R. McGuire, J. A. Aboaf, and E. Klokholm, *IEEE Trans. Magn.* **20**, 972 (1984).
- [12] M. Tsunoda, Y. Komasaki, S. Kokado, S. Isogami, C.-C. Chen, and M. Takahashi, *Appl. Phys. Express* **2**, 083001 (2009).
- [13] M. Ziese, *Phys. Rev. B* **62**, 1044 (2000).
- [14] E. Favre-Nicolin and L. Ranno, *J. Magn. Magn. Mater.* **272**, 1814 (2004).
- [15] H. Nakayama, M. Althammer, Y.-T. Chen, K. Uchida, Y. Kajiwara, D. Kikuchi, T. Ohtani, S. Geprägs, M. Opel, S. Takahashi, R. Gross, G. E. W. Bauer, S. T. B. Goennenwein, and E. Saitoh, *Phys. Rev. Lett.* **110**, 206601 (2013).
- [16] Y.-T. Chen, S. Takahashi, H. Nakayama, M. Althammer, S. T. B. Goennenwein, E. Saitoh, and G. E. W. Bauer, *Phys. Rev. B* **87**, 144411 (2013).
- [17] J. H. Han, C. Song, F. Li, Y. Y. Wang, G. Y. Wang, Q. H. Yang, and F. Pan, *Phys. Rev. B* **90**, 144431 (2014).
- [18] J. Kim, P. Sheng, S. Takahashi, S. Mitani, and M. Hayashi, *Phys. Rev. Lett.* **116**, 097201 (2016).
- [19] Z. Z. Luan, L. F. Zhou, P. Wang, S. Zhang, J. Du, J. Xiao, R. H. Liu, and D. Wu, *Phys. Rev. B* **99**, 174406 (2019).
- [20] Y. Yang, Z. Luo, H. Wu, Y. Xu, R.-W. Li, S. J. Pennycook, S. Zhang, and Y. Wu, *Nat. Commun.* **9**, 2255 (2018).
- [21] W. Zhou, T. Seki, T. Kubota, G. E. W. Bauer, and K. Takanashi, *Phys. Rev. Mater.* **2**, 094404 (2018).
- [22] M. Althammer, S. Meyer, H. Nakayama, M. Schreier, S. Altmannshofer, M. Weiler, H. Huebl, S. Geprägs, M. Opel, R. Gross *et al.*, *Phys. Rev. B* **87**, 224401 (2013).
- [23] W. Limmer, M. Glunk, J. Daeubler, T. Hummel, W. Schoch, R. Sauer, C. Bihler, H. Huebl, M. S. Brandt, and S. T. B. Goennenwein, *Phys. Rev. B* **74**, 205205 (2006).
- [24] L. K. Zou, Y. Zhang, L. Gu, J. W. Cai, and L. Sun, *Phys. Rev. B* **93**, 075309 (2016).
- [25] J. X. Li, M. W. Jia, Z. Ding, J. H. Liang, Y. M. Luo, and Y. Z. Wu, *Phys. Rev. B* **90**, 214415 (2014).
- [26] See Supplemental Material at <http://link.aps.org/supplemental/10.1103/PhysRevB.100.144425> for the proof of the amorphous multilayers, the magnetoresistance of CoFeB single layer, and the deduction of ρ_{AH} and R_{PHE} for Ta/Ir(t_{Ir})/CoFeB series samples.
- [27] S. Kokado, M. Tsunoda, K. Harigaya, and A. Sakuma, *J. Phys. Soc. Jpn.* **81**, 024705 (2012).
- [28] H. Gamou, Y. Du, M. Kohda, and J. Nitta, *Phys. Rev. B* **99**, 184408 (2019).
- [29] S. Cho, S.-h. C. Baek, K.-D. Lee, Y. Jo, and B.-G. Park, *Sci. Rep.* **5**, 14668 (2015).
- [30] F. Wilhelm, P. Pouloupoulos, H. Wende, A. Scherz, K. Baberschke, M. Angelakeris, N. K. Flevaris, and A. Rogalev, *Phys. Rev. Lett.* **87**, 207202 (2001).
- [31] R. Wienke, G. Schütz, and H. Ebert, *J. Appl. Phys.* **69**, 6147 (1991).
- [32] Z. Wei, M. B. Jungfleisch, J. Wanjun, J. Sklenar, F. Y. Fradin, J. E. Pearson, J. B. Ketterson, and A. Hoffmann, *J. Appl. Phys.* **117**, 172610 (2015).
- [33] T. White, T. Bailey, M. Pierce, and C. W. Miller, *IEEE Magn. Lett.* **8**, 3508304 (2017).
- [34] T. Tanaka, H. Kontani, M. Naito, T. Naito, D. S. Hirashima, K. Yamada, and J. Inoue, *Phys. Rev. B* **77**, 165117 (2008).
- [35] K.-S. Ryu, S.-H. Yang, L. Thomas, and S. S. P. Parkin, *Nat. Commun.* **5**, 3910 (2014).
- [36] H. L. Wang, C. H. Du, Y. Pu, R. Adur, P. C. Hammel, and F. Y. Yang, *Phys. Rev. Lett.* **112**, 197201 (2014).
- [37] L. J. Zhu, D. C. Ralph, and R. A. Buhrman, *Phys. Rev. Lett.* **122**, 077201 (2019).
- [38] B. F. Miao, L. Sun, D. Wu, C. L. Chien, and H. F. Ding, *Phys. Rev. B* **94**, 174430 (2016).
- [39] N. Nagaosa, J. Sinova, S. Onoda, A. H. MacDonald, and N. P. Ong, *Rev. Mod. Phys.* **82**, 1539 (2010).
- [40] J. Smit, *Physica* **21**, 877 (1955).
- [41] S. Iihama, T. Taniguchi, K. Yakushiji, A. Fukushima, Y. Shiota, S. Tsunegi, R. Hiramatsu, S. Yuasa, Y. Suzuki, and H. Kubota, *Nat. Electron.* **1**, 120 (2018).
- [42] V. L. Grigoryan, W. Guo, G. E. W. Bauer, and J. Xiao, *Phys. Rev. B* **90**, 161412(R) (2014).
- [43] L. Zhou, H. Song, K. Liu, Z. Luan, P. Wang, L. Sun, S. Jiang, H. Xiang, Y. Chen, J. Du, H. Ding, K. Xia, J. Xiao, and D. Wu, *Sci. Adv.* **4**, eaao3318 (2018).